Nuclear skin and the curvature of the symmetry energy

Ad. R. Raduta[1,*] and F. Gulminelli[2,†]
[1]*National Institute for Physics and Nuclear Engineering (IFIN-HH), RO-077125, Bucharest-Magurele, Romania*
[2]*Universite de Caen Normandie, ENSICAEN, LPC, UMR6534, F-14050 Caen, France*

(Received 16 December 2017; published 13 June 2018)

The effect of correlations between the slope and the curvature of the symmetry energy on ground-state nuclear observables is studied within the extended Thomas-Fermi approximation. We consider different isovector probes of the symmetry energy, with a special focus on the neutron skin thickness of ^{208}Pb. We use a recently proposed metamodeling technique to generate a large number of equation of state models, where the empirical parameters are independently varied. The results are compared to a set of calculations using 17 different Skyrme interactions. We show that the curvature parameter plays a non-negligible role on the neutron skin, while the effect is reduced in Skyrme functionals because of the correlation with the slope parameter.

DOI: 10.1103/PhysRevC.97.064309

I. INTRODUCTION

The determination of the nuclear matter equation of state (EoS) is an extremely lively issue in modern nuclear physics and astrophysics. The biggest uncertainties concern high density and strongly asymmetric matter, where the EoS determination is of outermost importance for the understanding of a large variety of astrophysical phenomena involving compact stars [1,2]. Observational measurements of neutron star mass and radii start to provide compelling constraints to the behavior of high-density matter [3,4], including the very recent multimessenger observation of a neutron star merger [5], where the EoS has a direct impact on the gravitational wave form mainly through the tidal polarizability parameter [6]. In this context, tight constraints coming from controlled nuclear experiments are extremely important, particularly concerning the isovector part of the EoS, the so-called symmetry energy [7,8]. A huge amount of literature is devoted to the determination of the symmetry energy at saturation ($E_{\rm sym}$) and its slope ($L_{\rm sym}$) by comparing selected isovector observables to EoS models issued from different energy density functionals (EDF) [9,10]. These studies have convincingly shown that a strong linear correlation exists between the $L_{\rm sym}$ parameter and the neutron skin thickness [11,12]. This latter can be measured directly from parity-violating electron scattering [13] and pion photoproduction [14] or probed via various isovector modes of collective excitations [15–20]. A good correlation is also typically observed with the $E_{\rm sym}$ parameter [21,22] and qualitatively explained by the fact that the behavior of the symmetry energy is, to a first-order approximation, linear in density in the subsaturation regime [23]. However, this correlation is somewhat blurred when different families of mean-field models are compared [24], showing that some residual model dependence exists. The careful study of Ref. [24] shows that this difference can be ascribed to different nucleon density distributions in the surface region. In turn, this can be due both to different surface properties of the functionals and to different behaviors of the symmetry energy at subsaturation, that is, to deviations from the linear approximation.

To progress on this issue, it is important to assess the role of the curvature of the symmetry energy ($K_{\rm sym}$) on isovector probes such as the nuclear skin. Little attention was paid to this parameter in the literature until recently [25,26], mainly due to the fact that it cannot be easily varied within a specific EoS model, because the functional form of the EoS imposes a correlation with the low order parameters $E_{\rm sym}$ and $L_{\rm sym}$. Still, if $K_{\rm sym}$ is of secondary role for nuclear structure observables, it is the main source of uncertainty when extrapolating the laboratory constraints to the high-density domain relevant for neutron star physics [27].

To perform this study, we use a recently proposed metamodeling approach to the EoS [28], where a large number of different EoS models can be generated without any *a priori* correlation among the different empirical parameters. Following Ref. [29], ground-state observables are calculated within the extended Thomas Fermi (ETF) approximation, with the addition of a gradient term as an effective parameter representing the different surface properties of the different models.

We show that the $K_{\rm sym}$ parameter plays a non-negligible role in the nuclear skin as well as in the differences of the proton radii of mirror nuclei and that the uncertainty on this parameter partially blurs the correlation with the symmetry energy slope.

The paper is organized as follows: The different energy functionals are briefly reviewed in Sec. II, as well as the ETF approximation used to calculate nuclear observables. In Sec. III, after discussing the overall performance of the ETF approximation on the Pb isotopic chain, we show our main results concerning the correlations between the different isovector observables and the empirical EoS parameters. Finally, conclusions are drawn in Sec. IV.

*araduta@nipne.ro
†gulminelli@lpccaen.in2p3.fr

II. FORMALISM

A. Skyrme EDF

The most extensive calculations of nuclear observables and their correlations with EoS parameters have been performed using Skyrme EDF [30].

The nuclear Skyrme energy density is expressed in terms of local nucleon densities $n_q(\boldsymbol{r})$, kinetic energy densities $\tau_q(\boldsymbol{r})$, and spin-orbit densities $\boldsymbol{J}_q(\boldsymbol{r})$ defined by [31]

$$n_q(\boldsymbol{r}) = \sum_{\nu,s} |\phi_\nu(\boldsymbol{r},s,q)|^2 n_\nu^q,$$

$$\tau_q(\boldsymbol{r}) = \sum_{\nu,s} |\nabla\phi_\nu(\boldsymbol{r},s,q)|^2 n_\nu^q,$$

$$\boldsymbol{J}_q(\boldsymbol{r}) = (-i) \sum_{\nu,s,s'} \phi_\nu^*(\boldsymbol{r},s',q)\nabla\phi_\nu(\boldsymbol{r},s,q) \times \langle s'|\sigma|s\rangle n_\nu^q, \quad (1)$$

where $\phi_\nu(\boldsymbol{r},s,q)$ represent the single-particle wave functions with orbital and spin numbers ν and s, $q = n,p$ indexes the nucleonic species, and n_ν^q are the occupation numbers. The functional form of the EDF is generated by a mean-field calculation with an effective zero-range momentum-dependent pseudopotential, augmented of a density-dependent term. Standard pseudopotentials, as the ones considered hereafter, depend on 10 parameters. The values of these parameters are typically determined by fits of experimental ground-state properties of spherical magic and semimagic nuclei (e.g., binding energy, root mean square (rms) radius of the charge distribution, spin-orbit splitting, isotope shifts, surface thickness, breathing mode energy, etc.) and/or properties of symmetric nuclear matter (energy $E_{\rm sat}$ and density $n_{\rm sat}$ at saturation, compression modulus $K_{\rm sat}$, symmetry energy $E_{\rm sym}$), and/or equation of state of pure neutron matter as predicted by *ab initio* models. These parameters vary largely from one Skyrme model to another. Properties of nuclear matter (NM) can be expressed analytically in terms of the same parameters [30].

In the following, 17 Skyrme EDFs will be employed: SKa [32], SKb [32], Rs [33], SkMP [34], SLy2 [35], SLy9 [35], SLy4 [36], SLy230a [37], SkI2 [38], SkI3 [38], SkI4 [38], SkI5 [38], SkI6 [39], SKOp [40], SK255 [41], SK272 [41], and KDE0v1 [42]. The extent to which they fulfill various constraints that have been obtained from experiment or microscopic calculations during the past decade [43] has been thoughtfully investigated in Ref. [44] in the context of unified equations of state for neutron star matter. Their values of saturation density of symmetric nuclear matter (SNM), energy per particle, and compression modulus of symmetric saturated matter span relatively narrow ranges, $0.1512 \leqslant n_{\rm sat} \leqslant 0.1646\,{\rm fm}^{-3}$, $-16.33 \leqslant E_{\rm sat} \leqslant -15.52$ MeV, and $222.40 \leqslant K_{\rm sat} \leqslant 271.5$ MeV, as these quantities are relatively well constrained. Larger domains are explored by the symmetry energy, $29.54 \leqslant E_{\rm sym} \leqslant 37.4$ MeV, and, especially, its slope and curvature $44.3 \leqslant L_{\rm sym} \leqslant 129.3$ MeV and $-127.2 \leqslant K_{\rm sym} \leqslant 159.5$ MeV.

It is worthwhile to notice that the functional form of the Skyrme energy density leads to correlations between the different EoS parameters. Indeed, five independent parameters govern the density dependence of the EDF (and two additional ones determine the density dependence of the effective masses). If the lowest order EoS parameters are fixed, namely $E_{\rm sat}$, $n_{\rm sat}$, $K_{\rm sat}$, $E_{\rm sym}$, $L_{\rm sym}$, the higher order parameters can be analytically expressed as a function of those fixed quantities. In particular, Skyrme EDFs show a clear correlation between the slope $L_{\rm sym}$ and the curvature $K_{\rm sym}$ of the symmetry energy at saturation, which are *a priori* independent EoS parameters.

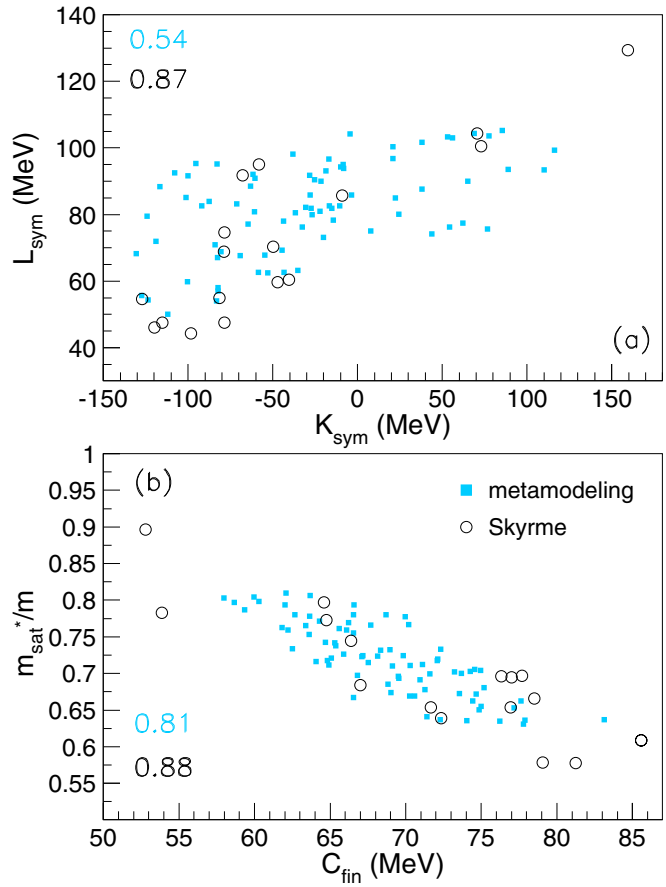

FIG. 1. Correlations between EoS parameters. Numbers on the left-hand side of each plot correspond to Pearson correlation coefficients between the parameters plotted on the axis. Upper (lower) values: meta-model (Skyrme).

This correlation, which obviously affects the extrapolation of the EoS to supersaturation densities, is graphically illustrated in the top panel of Fig. 1 (open circles). Its Pearson correlation coefficient[1] is $C(K_{\rm sym},L_{\rm sym}) = 0.87$. It was recently shown that this correlation is observed in a large class of functionals and might therefore be physically founded [25,26], even if its origin is not fully understood.

Another interesting nontrivial correlation is found between the effective nucleon mass at saturation, $m^*_{\rm sat}$, and the isoscalar-like finite-size parameter $C_{\rm fin}$ (see Sec. II B and Ref. [29]). This correlation is illustrated in the bottom panel of Fig. 1. Its Pearson correlation coefficient is $C(m^*_{\rm sat},C_{\rm fin}) = 0.88$. As already

[1]The Pearson correlation coefficient between two variables X and Y is defined by $C(X,Y) = (\langle XY\rangle - \langle X\rangle\langle Y\rangle)/\sigma(X)\sigma(Y)$.

discussed in Ref. [29], this correlation is probably induced by the parameter fitting protocol of Skyrme functionals. Indeed, $m^*_{\rm sat}$ and $C_{\rm fin}$ are related to nonlocal terms in the EDF which have an opposite effect on the surface energy, and neither of them plays a role in the determination of EoS parameters: For a given set of EoS parameters, a similar overall reproduction of binding energies over the nuclear chart can be obtained with compensating effects of the nonlocal terms.

B. Metamodeling of the EDF

A theoretical calculation of a nuclear observable depends, besides the EoS, on the functional form assumed for the EDF as well as on the many-body technique employed. To assess the model dependence due to the functional form of the EDF, one should consider different families of models with similar values for the EoS parameters. To this aim, a metamodeling technique was proposed in Ref. [28] and extended to finite nuclei EDF in Ref. [29]. By varying the parameters of the metamodeling, a large number of EoS from different families of mean-field EDF can be generated. Moreover, density dependencies that do not correspond to existing functionals but do not violate any empirical constraint can be also explored [28]. The inclusion of a single gradient term provides a minimal flexible EDF for finite nuclei, with performances on nuclear mass and radii comparable to the ones of full Skyrme functionals [29]. The exploration of the metamodeling parameter space thus allows a full estimation of the possible model dependence of the extraction of EoS parameters from nuclear ground-state observables, due to the choice of the EDF.

The potential energy per baryon is expressed as a Taylor expansion around saturation of symmetric nuclear matter in terms of the density parameter $x = (n - n_{\rm sat})/(3n_{\rm sat})$,

$$e_{\rm pot}(x,\delta) = \sum_{\alpha=0}^{N}(a_{\alpha 0} + a_{\alpha 2}\delta^2)\frac{x^\alpha}{\alpha!}u_\alpha(x)\,, \tag{2}$$

where the functions $u_\alpha(x)$ represent a low-density correction, ensuring a vanishing energy in the limit of vanishing density, without affecting the derivatives at saturation.

To correctly reproduce with a limited expansion order N existing nonrelativistic (Skyrme and *ab initio*) and relativistic (RMF and RHF) EDFs up to total densities $n = n_n + n_p \approx 0.6$ fm^{-3}, and isospin asymmetries $\delta = (n_n - n_p)/n$ ranging from symmetric matter $\delta = 0$ to pure neutron matter $\delta = 1$, the functional is supplemented by a kinetic-like term adding the expected $n^{2/3}$ dependence at low densities, as well as the contribution of higher orders in the δ expansion, as

$$e_{\rm kin}(x,\delta) = \frac{t^{FG}_{\rm sat}}{2}(1+3x)^{2/3}\left[(1+\delta)^{5/3}\frac{m}{m^*_n} + (1-\delta)^{5/3}\frac{m}{m^*_p}\right], \tag{3}$$

where $t^{FG}_{\rm sat} = (3\hbar^2)/(10m)(3\pi^2/2)^{2/3}n^{2/3}_{\rm sat}$ is the energy per nucleon of a free symmetric Fermi gas at nuclear saturation, m stands for the nucleon mass, and m^*_q denotes the effective mass of the nucleons $q = n, p$. For more details, see model ELFc in Ref. [28].

In the present work, we only consider subsaturation matter and, to avoid proliferation of unconstrained parameters, we limit the expansion to $N = 2$, which was shown to be enough to get a fair reproduction of nuclear masses [29]. The possible influence of higher order parameters is left for future work. When only average nuclear properties (e.g., binding energies and rms radii of neutron and proton distributions) are calculated, isoscalar and isovector finite-size and spin-orbit interactions can be fairly well described by a single isoscalar-like density gradient term [29] of the form $C_{\rm fin}(\nabla n_n + \nabla n_p)^2$. For the sake of convenience, only this isoscalar density gradient will be considered in this work. Following Ref. [29], we also neglect the effective mass splitting between neutrons and protons. The metamodeling parameters are then directly linked to the usual first- and second-order empirical parameters of the EoS by

$$a_{00} = E_{\rm sat} - t^{FG}_{\rm sat}(1+\kappa_{\rm sat}), \tag{4}$$

$$a_{10} = -t^{FG}_{\rm sat}(2+5\kappa_{\rm sat}), \tag{5}$$

$$a_{20} = K_{\rm sat} - 2t^{FG}_{\rm sat}(-1+5\kappa_{\rm sat}), \tag{6}$$

$$a_{02} = E_{\rm sym} - \tfrac{5}{9}t^{FG}_{\rm sat}(1+\kappa_{\rm sat}), \tag{7}$$

$$a_{12} = L_{\rm sym} - \tfrac{5}{9}t^{FG}_{\rm sat}(2+5\kappa_{\rm sat}), \tag{8}$$

$$a_{22} = K_{\rm sym} - \tfrac{10}{9}t^{FG}_{\rm sat}(-1+5\kappa_{\rm sat}), \tag{9}$$

where $\kappa_{\rm sat} = m/m^*_{\rm sat} - 1$.

Different EDF models for nuclei are generated by largely and evenly exploring the parameter space $\{P_\alpha\} = \{n_{\rm sat}, E_{\rm sat}, K_{\rm sat}, E_{\rm sym}, L_{\rm sym}, K_{\rm sym}, m^*_{\rm sat}, C_{\rm fin}\}$. For a given model, the ground-state nuclear energies and radii are calculated in the extended Thomas Fermi approximation at second order, as detailed in the next section. We retain for the subsequent analysis only the models $\{P_\alpha\}$ which provide a fair description of the experimental binding energies of the spherical magic nuclei, (40,20), (48,20), (48,28), (58,28), (88, 38), (90, 40), (114, 50), (132, 50), and (208, 82), and charge radii, (40,20), (48,20), (58,28), (88, 38), (90, 40), (114, 50), (132, 50), and (208, 82). The absence of the nucleus (48,28) in the second list is due to the fact that its experimental charge radius is not yet available. We recall that this set of data represents the core of nuclear properties on which the parameters of many Skyrme interactions have been fitted. The limitation to spherical nuclei is obviously due to the simplifying spherical approximation of most approaches, including ours. Specifically, retained EDFs correspond to sets of parameters $\{P_\alpha\}$ which provide $\chi(B) \leqslant 5$ MeV and $\chi(R_{\rm ch}) \leqslant 0.10$ fm. The minimum values here obtained for standard deviation of masses and charge radii are 2.7 MeV and, respectively, 2.07×10^{-2} fm. As usual in the literature, the χ^2 function is defined as $\chi^2(X) = \sum_{i=1}^{N}(X_{{\rm ETF}(i)} - X_{{\rm exp}(i)})^2/N$. The accepted values of standard deviation on mass are typically one order of magnitude larger than the lowest value in the literature, 0.5 MeV, which corresponds to more than 2350 nuclei and has been obtained in the framework of a Hartree-Fock-Bogoliubov (HFB) mass model [45].

The variation domain of each parameter is obtained by considering the dispersion of the corresponding values in a large number of relativistic and nonrelativistic mean-field models; see Ref. [28]. The precise frontiers of this domain depend on

TABLE I. Average and standard variation of the different parameters of the phenomenological EDF, calculated based on 51 Skyrme interactions and 15 relativistic mean-field interactions (see Table IV in Ref. [28]).

Parameter $\{P_\alpha\}$	n_{sat} (fm^{-3})	E_{sat} (MeV)	K_{sat} (MeV)	E_{sym} (MeV)	L_{sym} (MeV)	K_{sym} (MeV)	m^*_{sat}/m	C_{fin} ($MeVfm^5$)
Average $\langle\{P_\alpha\}\rangle$	0.1543	−16.03	251	33.30	76.6	−3	0.72	75
Standard deviation σ_α	±0.0054	±0.20	±29	±2.65	±29.2	±132	±0.09	±25

the number of models considered and their selection criteria and is therefore somewhat arbitrary. However, a variation of the borders of the parameter space might affect the overall dispersion in the predictions of the metamodel but not the quality of the correlations among parameters and observables, which is the scope of the present work.

The domain considered for each parameter P_α is reported in Table I in terms of average value and standard deviation. Good (poor) experimental constraints on n_{sat}, E_{sat}, and E_{sym} on one hand and K_{sat}, L_{sym}, and K_{sym} on the other hand lead to narrow (wide) variation domains of these variables.

As a first application of the metamodeling, we can investigate the model dependence of the correlations among empirical parameters observed in the previous section for the Skyrme EDFs.

The only significant correlation that was found in the different models generated by the metamodeling technique after application of the mass and radius filter is the one between m^*_{sat} and C_{fin}, as shown by solid squares in the bottom panel of Fig. 1. The value of the correlation coefficient, $C = 0.81$, is close to our previous calculations using a simplified version of the extended Thomas Fermi approach [29] and also to the correlation coefficient of Skyrme pseudopotentials. This confirms that the Skyrme correlation comes from the physical constraint of mass reproduction and is largely independent of the EDF model.

Conversely, only a poor correlation between L_{sym} and K_{sym} emerges from the metamodeling after application of the mass constraint; see solid squares in the top panel of Fig. 1. This suggests that the origin of that correlation observed in different functionals [25,26] is not due to the constraint of mass reproduction.

C. The Extended Thomas-Fermi approximation with parametrized density profiles

For a given EDF model, average properties of atomic nuclei can be reasonably well described within the extended Thomas-Fermi (ETF) approximation [46]. In this work, we will limit ourselves to the second-order expansion in $\hbar$ and to parametrized density profiles in spherical symmetry, such as to limit the number of variational parameters. Because of these approximations, the degree of reproduction of experimental data is not comparable to the one of dedicated fully quantal HFB calculations [45], and more realistic calculations will definitely have to be performed in order to determine EoS parameters in a fully quantitative way. Still, the complete exploration of the parameter space is not affordable with these more sophisticated many-body techniques, and we believe that an ETF metamodeling is sufficient to extract the correlations between EoS parameters and the neutron skin.

In the ETF framework, the energy of an arbitrary distribution of nucleons with densities $\{n_n(\boldsymbol{r}),n_p(\boldsymbol{r})\}$ is given by the volume integral of the energy density according to

$$E_{tot} = \int d\boldsymbol{r}(e_{nuc}[n_n,n_p] + e_{Coul}[n_p]), \tag{10}$$

where the first term stands for the nuclear energy and the second stands for the electrostatic contribution.

At second order in the $\hbar$ expansion, the nuclear energy density functional writes

$$e_{nuc}[n_n,n_p] = \sum_{q=n,p} \frac{\hbar^2}{2m^*_q}\tau_{2q} + e_{TF}, \tag{11}$$

where e_{TF} is the Thomas-Fermi approximation of the chosen nuclear EDF model, which can depend on local densities n_q as well as on density gradients ∇n_q and currents $\boldsymbol{J}_q$ and τ_{2q} is the (local and nonlocal) density-dependent correction arising from the second-order $\hbar$ expansion of the kinetic energy density operator.

The Coulomb energy density is expressed as [47]

$$e_{Coul}[n_p] = \frac{e^2}{2}n_p(\boldsymbol{r})\int \frac{n_p(\boldsymbol{r'})}{|\boldsymbol{r}-\boldsymbol{r'}|}d\boldsymbol{r'} - \frac{3e^2}{4}\left(\frac{3}{\pi}\right)^{1/3} n_p^{4/3}(\boldsymbol{r}), \tag{12}$$

where the Slater approximation has been employed to estimate the exchange Coulomb energy density.

The ground state is determined by energy minimization using parametrized neutron and proton distributions. For a generic nucleus with N neutrons and Z protons and under the simplifying approximation of spherical symmetry, these are customarily parametrized as Wood-Saxon (WS) density profiles,

$$n_q^{WS}(r) = \frac{n_{bulk,q}}{1+\exp\left[\left(r-R_q^{WS}\right)/a_q\right]}, \tag{13}$$

where $n_{bulk,q}$ is linked to the central density of the $q = n,p$ distribution, and R_q^{WS} and a_q respectively stand for radius and diffuseness parameters. With the extra condition of particle number conservation,

$$Z = 4\pi\int_0^\infty drr^2 n_p(r), N = 4\pi\int_0^\infty drr^2 n_n(r), \tag{14}$$

only four variables out of six are independent. In the variational calculation of the ground state, we make the choice of varying $\{n_{bulk,q},a_q; q = n,p\}$, while R_q^{WS} are obtained from Eq. (14).

The only experimental observables related to the distribution of matter are the root mean squared (rms) radius of the

charge distribution and, with larger error bars, neutron skin thickness. Rms radius of the charge distribution is defined as the rms radius of the proton distribution corrected for the internal charge distribution of the proton $S_p = 0.8$ fm,

$$\langle r_{ch}^2 \rangle^{1/2} = \left[\langle r_p^2 \rangle + S_p^2 \right]^{1/2}. \tag{15}$$

Neutron skin thickness is defined as the difference in the neutron-proton rms radii,

$$\Delta r_{np} = \langle r_n^2 \rangle^{1/2} - \langle r_p^2 \rangle^{1/2}, \tag{16}$$

and, as demonstrated in Ref. [24], it can be decomposed with good accuracy into a bulk contribution,

$$\Delta r_{np}^{\rm bulk} = \sqrt{\frac{3}{5}} \left[\left(R_n^{WS} - R_p^{WS} \right) + \frac{\pi^2}{3} \left(\frac{a_n^2}{R_n^{WS}} - \frac{a_p^2}{R_p^{WS}} \right) \right], \tag{17}$$

and a surface contribution,

$$\Delta r_{np}^{\rm surf} = \sqrt{\frac{3}{5}} \frac{5\pi^2}{6} \left(\frac{a_n^2}{R_n^{WS}} - \frac{a_p^2}{R_p^{WS}} \right). \tag{18}$$

It is worthwhile to notice that each of these contributions depends on both WS radii and diffusivities of neutron and proton distributions.

III. RESULTS

A. Performance of the ETF approximation on experimental data

In order to visualize the overall performance of the ETF approximation, we consider in this section a single nuclear EDF model, namely the SLy4 [36] functional. We note that a lot of data on which SLy4 [36] has been constrained includes binding energies and rms radii of doubly magic nuclei and the equation of state of pure neutron matter of Ref. [48]. The last constraint guarantees a correct behavior at high isospin asymmetry.

In terms of average standard deviation on masses and radii, we obtain for the considered pool of spherical nuclei $\chi(B) = 4.9$ MeV and $\chi(R_{\rm ch}) = 4.1 \times 10^{-2}$ fm.

The results of total, i.e., nuclear plus electrostatic, energy minimization in the four-dimensional space $\{n_{{\rm bulk},n}, n_{{\rm bulk},p}, a_n, a_p\}$ are plotted in Figs. 2 and 3 for the isotopic chain of Pb as a function of the isospin asymmetry, $I = 1 - 2Z/A$. Two different methods are used to calculate the Coulomb energy. In one case, it is calculated by accounting for the diffusivity of the proton distribution via Eq. (12) ("self-consistent"). In the second, a uniformly charge distribution approximation is employed, which leads to $0.69Z^2/A^{1/3}$ ("approx."). The top and middle panels of Fig. 2 present the evolution of each of the four variational parameters as a function of I. The bottom panel presents the I dependence of the WS radii on neutron and proton distributions, obtained from particle number conservation. We notice the important effect of a self-consistent treatment of Coulomb in the determination of the density profiles. In particular, the obtained bulk densities and diffuseness parameters are in good agreement with fits of HF density profiles with the same EDF [49], which reassures us of the quality of the approximation.

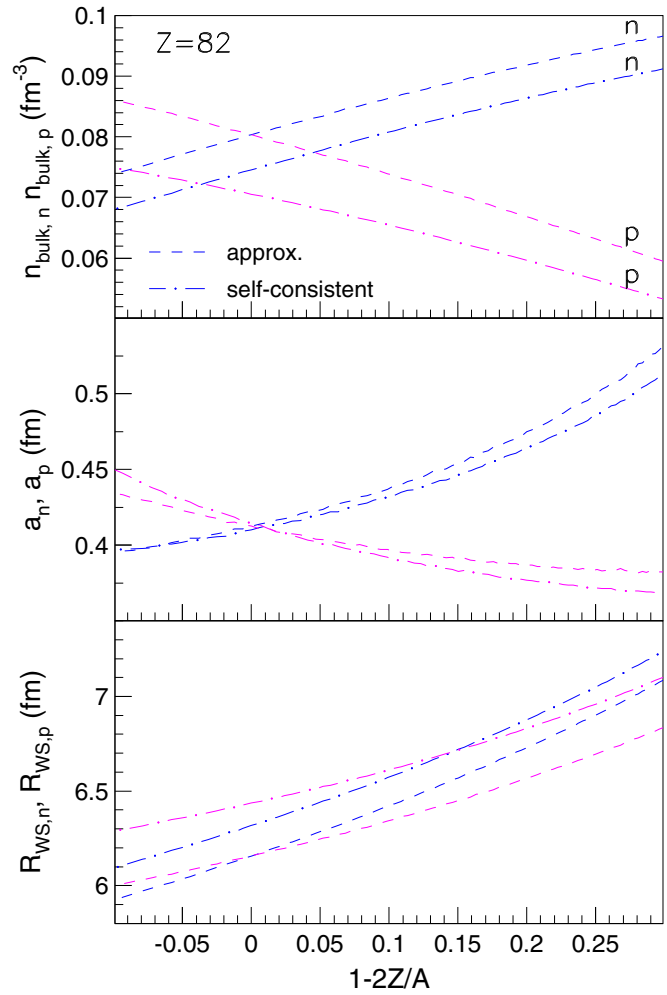

FIG. 2. ETF results corresponding to the ground state of Pb isotopes, for a representative EDF model (SLy4 [36]). Variational parameters $n_{{\rm bulk},n}$, $n_{{\rm bulk},p}$ (top panel), a_n, a_p (middle panel), and R_n^{WS} and R_p^{WS} (bottom panel) are plotted as a function of total isospin asymmetry. The results obtained by considering the diffusivity of the charge distribution ["self-consistent," Eq. (12)] are confronted with those corresponding to the uniformly charged sphere approximation ("approx.").

We can also see that WS radii of neutron and proton distributions have similar values, though strongly dependent on I. This might suggest that the skin is mainly a surface effect for this calculation. However, this interpretation is not correct because the equivalent sharp radius $R_q^3 = [3 \int dr r^2 n_q(r)]/n_{{\rm bulk},q}$ is different from the WS radius parameter, R_q^{WS}, and effectively depends on the diffuseness of the profile [24]. Moreover, as explicitly worked out in Ref. [50], the diffuseness parameter itself depends in a highly nontrivial way both on the gradient terms of the EDF and on the bulk properties of matter.

Figure 3 illustrates the total binding energy per nucleon (top panel), rms radius of charge distribution (middle panel), and neutron skin thickness (lower panel) as a function of I. When available, experimental data for binding energies [51]

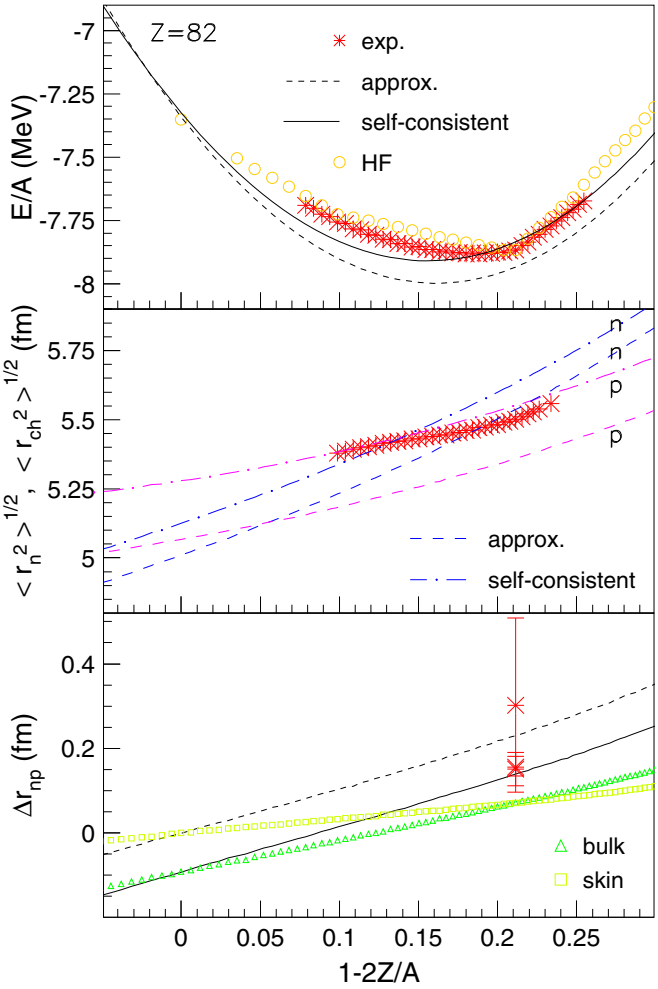

FIG. 3. ETF results corresponding to the ground state of Pb isotopes and SLy4 [36]. Binding energy per nucleon (top panel), rms radii of neutron and charge distributions (middle panel), and neutron skin thickness are plotted as a function of total isospin asymmetry. When available, experimental masses [51] and charge radii [52] are plotted as well. For neutron skin thicknesses of ^{208}Pb, the following experimental data are illustrated: 0.1515 ± 0.0197 fm [15], $0.156^{+0.025}_{-0.021}$ fm [16], and $0.3012 \pm (0.175)_{\rm exp} \pm (0.026)_{\rm model} \pm (0.005)_{\rm strange}$ fm [13,53]. As in Fig. 2, two methods for calculating the Coulomb energy are considered. Neutron skin thickness decomposition into bulk and surface contributions according to Eqs. (17, 18) is represented on the bottom panel for the case in which the Coulomb energy is calculated self-consistently (open symbols).

and charge radii [52] are plotted as well. For neutron skin thickness of ^{208}Pb, we display data from Refs. [13,15,16,53]. Self-consistent calculation of the Coulomb energy leads to a fair agreement with experimental data though a systematic overbinding is obtained for nuclei with $I < 0.17$. Complete HF calculations from Ref. [29], performed in spherical symmetry, are also shown. Aside from a residual deviation which can be ascribed to the choice of the functional and/or beyond mean-field effects, HF calculation describe very well the experimental data. Concerning the ETF calculations, we can see that missing higher $\hbar$ orders and the use of a parametrized density profiles lead to a deviation with respect to the experimental data, which is larger than that of the HF calculation. The energy error is, however, very small for ^{208}Pb and neighboring nuclei. This justifies the method described in Sec. II B and employed to build metamodeling EDF based on best fit of properties of spherical nuclei.

The performances of the ETF approximation when Coulomb is consistently included in the variation can be judged also from the agreement of rms radii of charge distributions with experimental data. As one may see in the middle panel of Fig. 3, the overall accord is good. The most important deviations, of the order of 0.05 fm, are obtained for $I > 0.17$. This deviation is comparable to the one obtained with complete ETF or DFT calculations in the absence of deformation [54,55] and can be ascribed to the choice of the functional and/or to beyond-mean-field effects. Neutron skin thickness presents a linear dependence on I irrespective of how Coulomb was calculated. As is easy to anticipate, the consistent displacement of neutron and proton distributions, due to the Coulomb repulsion, leads to values of the neutron skin thickness lower than those obtained in the simplifying approximation. It is interesting to remark that while the Coulomb effect decreases the neutron skin, the different diffuseness of the proton and neutron density profiles tends to increase it. As a consequence, the two effects partially cancel and the global result is close to our previous calculations [29], where both effects were neglected in order to obtain analytic approximations. The bottom panel depicts also the bulk and surface contribution to the skin thickness [24], calculated according to Eqs. (17) and (18). One notices that, for ^{208}Pb, they contribute equally to the total thickness while in neutron-richer (neutron-poorer) isotopes it is the bulk (surface) term that dominates. Given the relatively low $L_{\rm sym} = 46$ MeV value of SLy4 [36], this result is in good agreement with the droplet model (DM) calculations of Ref. [56], where the dominance of bulk or surface contributions was shown to be linked to the value of $L_{\rm sym}$.

B. Correlations between nuclear observables and parameters of nuclear matter

The correlation between the neutron skin thickness of ^{208}Pb and $L_{\rm sym}$ has been reported in the past years in many different studies based on density functionals [11,12,24], semiclassical approaches [56,57], and DM [56].

More recently, the existence of other correlations with various isovector modes of collective excitation was suggested, namely electric dipole polarizability [16–18], isovector giant dipole resonance (IVGDR) [58], isovector giant quadrupole resonance (IVGQR) [20], pygmy dipole resonance (PDR) [19,58,59], and antianalog giant dipole resonance (AGDR) [60–62]. A correct description of these modes demands a dynamical treatment in the framework of linear response theory and is beyond the purpose of this work. However, simplified expressions were proposed. An example in this sense is given by Ref. [63], which relates the electric dipole polarizability of a nucleus of mass number A and isospin asymmetry I,

$$\alpha_D = \frac{\pi e^2}{54}\frac{A\langle r^2\rangle}{E_{\rm sym}}\left(1+\frac{5}{3}\frac{E_{\rm sym}-a_{\rm sym}}{E_{\rm sym}}\right), \qquad (19)$$

with the ground-state symmetry energy in the local density approximation [24]

$$a_{\rm sym}(A) = \frac{4\pi}{AI^2}\int_0^\infty dr\, r^2 n(r)\delta^2(r) e_{\rm sym}[n(r)], \qquad (20)$$

where $e_{\rm sym} = (1/2)\partial^2 e(n,\delta)/\partial\delta^2|_{\delta=0}$ represents the local symmetry energy. Another example is offered by Ref. [64] which expresses the IVGDR energy constant in terms of symmetry energy, saturation density, and surface stiffness coefficient, $Q_{\rm stiff}$, as

$$D = D_\infty/\sqrt{1 + 3E_{\rm sym}A^{-1/3}/Q_{\rm stiff}}, \qquad (21)$$

where $D_\infty = \sqrt{8\hbar^2 E_{\rm sym}/(mr_0^2)}$ and $r_0^3 = 3/(4\pi n_{\rm sat})$. The surface stiffness coefficient measures the resistance of the asymmetric semi-infinite nuclear matter against separation of neutrons and protons to form a skin and is typically performed within HF or ETF approaches. Such calculations showed some sensitivity of $Q_{\rm stiff}$ to the calculation procedure [65,66] as well as significant correlations with the symmetry energy and its first- and second-order derivatives [57,67]. Different approximation formulas have been proposed. Some of them express $Q_{\rm stiff}$ in terms of a number of nuclear matter parameters and are based on fits of HF or ETF calculations performed using different EDFs. Within the liquid drop model, Ref. [46] calculates $Q_{\rm stiff}$ from calculations of finite nuclei disregarding the Coulomb interaction. In the present work, we adopt the expression, $Q_{\rm stiff} = 9E_{\rm sym}A^{-1/3}/4/(E_{\rm sym}/a_{\rm asym} - 1)$, obtained by equating the ground-state symmetry energy given by Eq. (20) with the corresponding DM expression [24]. For the case of ^{208}Pb, its accuracy is of the order of 10%, which leads to a relative error of 2% on the IVGDR energy constant of ^{208}Pb calculated according to Eq. (21). This small uncertainty only marginally affects the correlation between the macroscopically derived IVGDR energy constant and various properties associated with the finite nuclei or the nuclear matter. However, more important distortions might come from the nature of the approximation itself, namely the use of macroscopic expressions in case of dynamical quantities. Such distortions apply to both α_D and D.

Another interesting observable, potentially linked to the isovector EoS parameters, is given by the difference between the proton radii $R_p = \langle r_p^2\rangle^{1/2}$ of mirror nuclei [68,69]. This observable has the interesting feature of being directly accessible from a variational calculation without any extra model assumption. Moreover, it is much more accessible experimentally than the neutron skin, which demands the measurement of the neutron distribution.

The correlation between the proton radii differences in mirror nuclei and electric dipole polarizability on one hand and neutron skin thicknesses on the other hand has been addressed in Refs. [23,68–70]. Reference [64] focused on the nuclear symmetry energy dependence of the IVGDR energies by considering a series of Skyrme interaction potentials. The correlations between neutron skin thickness, electric dipole polarizability, and IVGDR energy constant of ^{208}Pb and proton radii difference for $A = 48$ mirror nuclei are investigated in Fig. 4 for both metamodeling EDF and Skyrme functional.

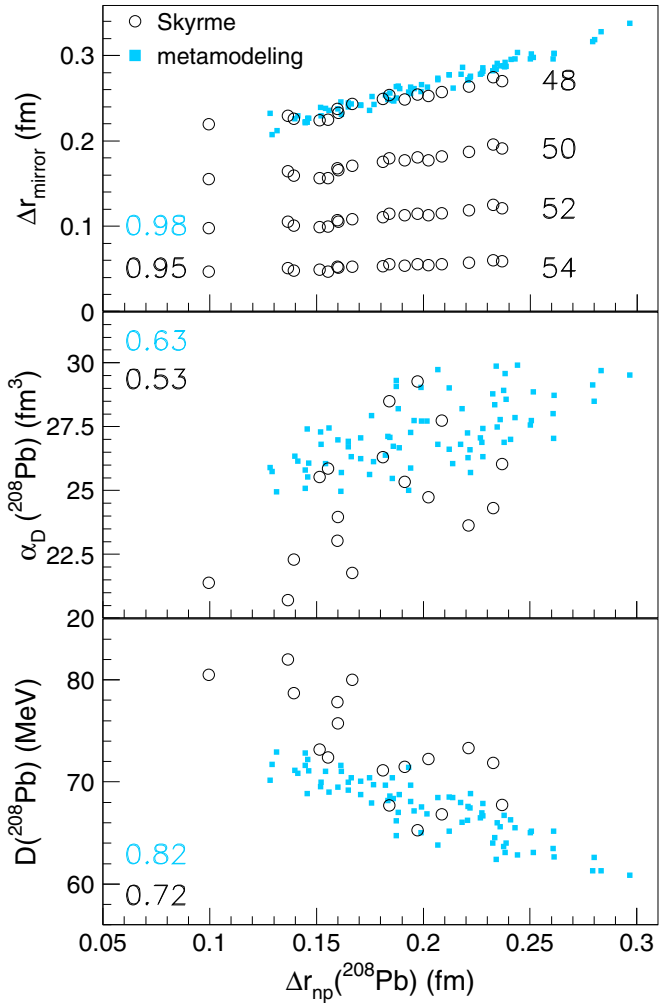

FIG. 4. Correlations between neutron skin thickness in ^{208}Pb and differences in the proton radii of mirror nuclei $R_p(^{48}\rm Ni) - R_p(^{48}\rm Ca)$ (top), electric dipole polarizability of ^{208}Pb (middle), and IVGDR energy constant of ^{208}Pb (bottom). Results corresponding to Skyrme and metamodeling are represented with open circles and, respectively, solid squares. Skyrme predictions corresponding to differences in the proton radii of mirror nuclei $R_p(^{50}\rm Ni) - R_p(^{50}\rm Ti)$, $R_p(^{52}\rm Ni) - R_p(^{52}\rm Cr)$, $R_p(^{54}\rm Ni) - R_p(^{54}\rm Fe)$ are also plotted in the top panel. Numbers on the left hand side of each plot correspond to Pearson correlation coefficients between the observables plotted on the axis. Upper (lower) values: metamodeling (Skyrme).

For completeness, Skyrme predictions corresponding to differences in the proton radii of $A = 50,52,54$ and $\Delta r_{np}(^{208}\rm Pb)$ are also plotted in the top panel. In the case of $\Delta r_{\rm mirror}$ vs $\Delta r_{np}(^{208}\rm Pb)$, metamodeling EDF leads to a strong correlation, with a Pearson correlation coefficient of 0.98. A moderate correlation is obtained for $D(^{208}\rm Pb)$ vs $\Delta r_{np}(^{208}\rm Pb)$. A poor correlation is found between the dipole polarizability and neutron skin thickness. Skyrme functionals provide very similar results. Very strong correlations are obtained only between $\Delta r_{np}(^{208}\rm Pb)$ and proton radii differences in mirror nuclei with $A = 48,50,52,54$. This result is in agreement with Refs. [68,69]. The correlation between electric dipole polarizability and $\Delta r_{np}(^{208}\rm Pb)$ is loose, in agreement with Ref. [70]. Reference [70] has actually evidenced that a much better

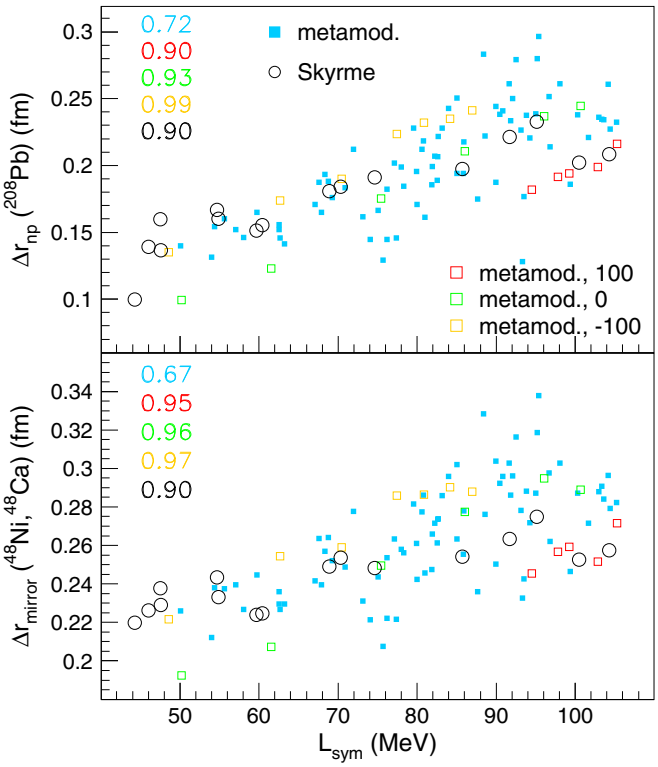

FIG. 5. Correlations between $L_{\rm sym}$ and $\Delta r_{np}(^{208}\mathrm{Pb})$ (top panel) and $L_{\rm sym}$ and $R_p(^{48}\mathrm{Ni}) - R_p(^{48}\mathrm{Ca})$ (bottom panel). In addition to metamodeling EDF plotted in the previous figures, here we consider also metamodeling EDF with fixed values of $K_{\rm sym} = 100, 0, -100$ MeV. The numbers on the left-hand side mention the Pearson correlation coefficients in the following order: metamodeling with freely varying $K_{\rm sym}$, metamodeling with $K_{\rm sym} = 100, 0, -100$ MeV, and Skyrme.

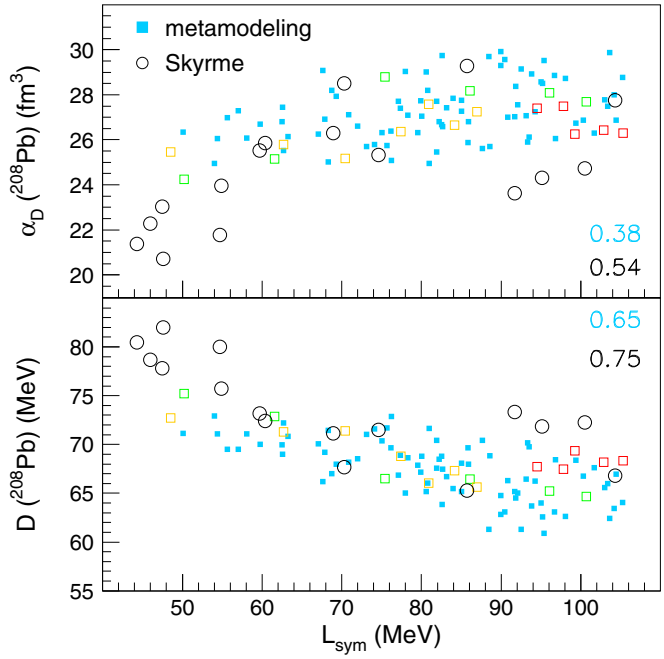

FIG. 6. Correlations between $L_{\rm sym}$ and $\alpha_D(^{208}\mathrm{Pb})$ (top) and $L_{\rm sym}$ and $D(^{208}\mathrm{Pb})$ (bottom). Numbers on the right-hand side of each plot correspond to Pearson correlation coefficients between the observables plotted on the axis. Upper (lower) values: metamodeling (Skyrme). As in Fig. 5, metamodeling EDF with fixed values of $K_{\rm sym} = 100, 0, -100$ MeV are plotted as well.

correlation holds between Δr_{np} and $(\alpha_D E_{\rm sym})$, as expected from Eq. (19). Finally Skyrme functionals lead to medium-strength correlations between the IVGDR energy constant and neutron skin thickness of ^{208}Pb. This result can be understood considering the $L_{\rm sym}$ and $K_{\rm sym}$ dependences of the D quantity via $Q_{\rm stiff}$.

We now turn to test the sensitivity of the observables to the different isovector parameters of the EoS. In a previous work [29], a full Bayesian analysis of the correlation matrix was performed, though with a more simplified version of the ETF metamodeling, which did not include the self-consistent treatment of Coulomb nor the definition of $(n_{\mathrm{bulk},n}, n_{\mathrm{bulk},p}, a_n, a_p)$ as independent variational variables. In that study, it was shown that the neutron skin is only sensitive to the $L_{\rm sym}$ parameter. The present calculations, with a more sophisticated treatment of the ETF metamodeling, confirm the results of our previous work.

The correlation between the neutron skin in ^{208}Pb and the $L_{\rm sym}$ parameter is shown in the top panel of Fig. 5. The lower value of the correlation coefficient with respect to the results of Ref. [29] can be understood from the fact that the difference between the neutron and proton diffusivity was neglected in Ref. [29]. This value is also lower than the one corresponding to Skyrme functionals, as well as the ones reported by most analyses in the literature using specific energy functionals [23,24,56,57,71]. The higher dispersion of the metamodeling is due to the fact that the different EoS parameters are fully independent in the metamodeling approach. As already observed in Ref. [29], though the EoS parameters are all influential in the calculation of nuclear masses and radii, the constraint on those quantities does not generate correlations among the EoS parameters because compensations can freely occur.

To demonstrate this statement, we have generated models with arbitrary fixed values of $K_{\rm sym}$ fulfilling the same criteria imposed to the global set of models; see Sec. II B. The resulting correlations are shown in Fig. 5 for three cases $K_{\rm sym} = -100, 0, 100$ MeV. We can observe that the correlation between ^{208}Pb and $L_{\rm sym}$ is greatly improved when $K_{\rm sym}$ is fixed. In the case of Skyrme functionals, $K_{\rm sym}$ can largely vary but its value is positively correlated to $L_{\rm sym}$ because of the specific function form of the density-dependent term in Skyrme interactions [see Fig. 1 (a)]. As a consequence, the Skyrme results interpolate the more general metamodel ones and the correlation coefficient is only slightly less than those corresponding to metamodel EDF with fixed $K_{\rm sym}$ values.

The bottom panel of Fig. 5 summarizes the analyses done above but for the correlation between the proton radii difference in $A = 48$ mirror nuclei and $L_{\rm sym}$. The conclusions are similar: Strong (poor) correlations exist in the case of Skyrme functionals and metamodeling EDF with fixed $K_{\rm sym}$ values (metamodeling EDF with freely varying $K_{\rm sym}$).

The correlations of the dipole polarizability and IVGDR energy constant of ^{208}Pb with $L_{\rm sym}$ are reported in Fig. 6, for the metamodeling and for the selected Skyrme functionals. As in Fig. 5, metamodeling EoS with fixed values of

$K_{\rm sym} = -100, 0, 100$ MeV are also considered. As one may see, $\alpha_D(^{208}\text{Pb})$ and $D(^{208}\text{Pb})$ show less correlation with $L_{\rm sym}$ than with $\Delta r_{np}(^{208}\text{Pb})$, when metamodeling EDF are employed. At variance with this, Skyrme functionals provide for $\alpha_D(^{208}\text{Pb})$ and $D(^{208}\text{Pb})$ almost the same degree of correlation with $L_{\rm sym}$ as with the neutron skin of ^{208}Pb. A word of caution is nevertheless in order. The accurate calculation of these two dynamical quantities is possible only within the linear response theory. Equations (19) and (21) presently employed rely on approximations and are thus are expected to distort the sensitivity to nuclear matter EoS.

In Ref. [29], the isoscalar and isovector parameters of the metamodelling EDF have been determined by fits of experimental binding energies of symmetric nuclei with masses $20 \leqslant A \leqslant 100$ and full isotopic chains of Ca, Ni, Sn, and Pb. We have tested that the conclusions drawn above and the degrees of correlation remain the same if the pool of nuclei on which the parameters of the EDF are determined is replaced by the one considered in Ref. [29].

IV. CONCLUSIONS

In this paper, we have explored the influence of the different isovector empirical EoS parameters on some properties of atomic nuclei, namely neutron skin thickness, difference in proton radii of mirror nuclei, dipole polarizability, and the IVGDR energy constant of ^{208}Pb.

The analysis was done within a recently proposed metamodeling technique [28,29]. Varying the parameters of the metamodeling, it is possible to reproduce existing relativistic and nonrelativistic EDF, as well as to consider novel density dependencies which are not explored by existing functionals. With respect to our previous work, Ref. [29], we have improved the ETF formalism employed to extract nuclear masses and radii out of a given EDF: The Coulomb interaction is consistently included in the variational procedure, and the bulk densities and diffuseness parameters of the density profiles are treated as independent variational parameters. These improvements allow a better description of nuclear radii and the nuclear skin. The correlation between this latter observable and the slope of the symmetry energy $L_{\rm sym}$, already reported in numerous studies in the literature with different EDFs as well as many-body techniques, is confirmed by our study.

However, we show that the quality of this correlation is considerably worsened if we allow independent variations of the curvature parameter $K_{\rm sym}$ with respect to the slope $L_{\rm sym}$, while this was not observed in previous studies, probably because in most existing functionals such correlation exists. We conclude that it will be very important to constrain the curvature parameter with dedicated studies, in order to reduce the confidence intervals of EoS parameter and allow more reliable extrapolations to the higher density domain.

We have shown that the condition of a reasonable reproduction of nuclear masses and radii does not necessarily imply any strong correlation between $L_{\rm sym}$ and $K_{\rm sym}$. For this reason, it is possible that the existing correlation in the Skyrme EDF might be spuriously induced by the arbitrariness of the functional form, particularly the density-dependent term. However, as suggested in Refs. [25,26], such a correlation might also be physical and linked to the fact that Skyrme EDF are derived from a pseudopotential which satisfies some basic physical properties, which is not the case of the more general metamodeling. To answer this question, it will be important to evaluate and possibly constrain this correlation on *ab initio* calculations of neutron matter [26]. This work is presently in progress.

[1] M. Oertel, M. Hempel, T. Klahn, and S. Typel, Rev. Mod. Phys. **89**, 015007 (2017).
[2] J. Lattimer, Annu. Rev. Nucl. Part. Sci. **62**, 485 (2012).
[3] A. W. Steiner, J. M. Lattimer, and E. F. Brown, Eur. Phys. J. A **52**, 18 (2016).
[4] J. M. Lattimer and A. W. Steiner, Eur. Phys. J. A **50**, 40 (2014).
[5] B. P. Abbott, R. Abbott, T. D. Abbott, F. Acernese, K. Ackley, C. Adams, T. Adams, P. Addesso, R. X. Adhikari, V. B. Adya *et al.*, Astrophys. J. Lett. **848**, L12 (2017).
[6] A. W. Steiner, S. Gandolfi, F. J. Fattoyev, and W. G. Newton, Phys. Rev. C **91**, 015804 (2015).
[7] B.-A. Li, À. Ramos, G. Verde, and I. Vidaña, Topical issue on the nuclear symmetry energy, Eur. Phys. J. A **50**, 9 (2014).
[8] J. M. Lattimer and M. Prakash, Phys. Rep. **621**, 127 (2016).
[9] M. B. Tsang, J. R. Stone, F. Camera, P. Danielewicz, S. Gandolfi, K. Hebeler, C. J. Horowitz, J. Lee, W. G. Lynch, Z. Kohley *et al.*, Phys. Rev. C **86**, 015803 (2012).
[10] M. Kortelainen, J. McDonnell, W. Nazarewicz, P.-G. Reinhard, J. Sarich, N. Schunck, M. V. Stoitsov, and S. M. Wild, Phys. Rev. C **85**, 024304 (2012).
[11] R. J. Furnstahl, Nucl. Phys. A **706**, 85 (2002).
[12] X. Roca-Maza, M. Centelles, X. Vinas, and M. Warda, Phys. Rev. Lett. **106**, 252501 (2011).
[13] S. Abrahamyan, Z. Ahmed, H. Albataineh, K. Aniol, D. S. Armstrong, W. Armstrong, T. Averett, B. Babineau, A. Barbieri, V. Bellini *et al.* (PREX Collaboration), Phys. Rev. Lett. **108**, 112502 (2012).
[14] C. M. Tarbert, D. P. Watts, D. I. Glazier, P. Aguar, J. Ahrens, J. R. M. Annand, H. J. Arends, R. Beck, V. Bekrenev, B. Boillat *et al.* (Crystal Ball at MAMI and A2 Collaboration), Phys. Rev. Lett. **112**, 242502 (2014).
[15] A. Trzcinska, J. Jastrzebski, P. Lubinski, F. J. Hartmann, R. Schmidt, T. von Egidy, and B. Klos, Phys. Rev. Lett. **87**, 082501 (2001).
[16] A. Tamii, I. Poltoratzka, P. Von-Neumann Cosel, Y. Fujita, T. Adachi, C. A. Bertulani, J. Carter, M. Dozono, H. Fujita, K. Fujita *et al.*, Phys. Rev. Lett. **107**, 062502 (2011).
[17] D. M. Rossi, P. Adrich, F. Aksouh, H. Alvarez-Pol, T. Aumann, J. Benlliure, M. Bohmer, K. Boretzky, E. Casarejos, M. Chartier *et al.*, Phys. Rev. Lett. **111**, 242503 (2013).
[18] J. Birkhan, M. Miorelli, S. Bacca, S. Bassauer, C. A. Bertulani, G. Hagen, H. Matsubara, P. von Neumann-Cosel, T. Papenbrock,

N. Pietralla, V. Yu. Ponomarev, A. Richter, A. Schwenk, and A. Tamii, Phys. Rev. Lett. **118**, 252501 (2017).
[19] A. Carbone, G. Colo, A. Bracco, L.-G. Cao, P. F. Bortignon, F. Camera, and O. Wieland, Phys. Rev. C **81**, 041301 (2010).
[20] S. S. Henshaw, M. W. Ahmed, G. Feldman, A. M. Nathan, and H. R. Weller, Phys. Rev. Lett. **107**, 222501 (2011).
[21] W. Nazarewicz, P.-G. Reinhard, W. Satula, and D. Vretenar, Eur. Phys. J. A **50**, 20 (2014).
[22] M. C. Papazoglou and Ch. C. Moustakidis, Phys. Rev. C **90**, 014305 (2014).
[23] X. Roca-Maza, N. Paar, and G. Colo, J. Phys. G **42**, 034033 (2015).
[24] C. Mondal, B. K. Agrawal, M. Centelles, G. Colo, X. Roca-Maza, N. Paar, X. Vinas, S. K. Singh, and S. K. Patra, Phys. Rev. C **93**, 064303 (2016).
[25] C. Mondal, B. K. Agrawal, J. N. De, S. K. Samaddar, M. Centelles, and X. Vinas, Phys. Rev. C **96**, 021302 (2017).
[26] I. Tews, J. M. Lattimer, A. Ohnishi, and E. E. Kolomeitsev, Astrophys. J. **848**, 105 (2017).
[27] J. Margueron, R. Hoffmann Casali, and F. Gulminelli, Phys. Rev. C **97**, 025806 (2018).
[28] J. Margueron, R. Hoffmann Casali, and F. Gulminelli, Phys. Rev. C **97**, 025805 (2018).
[29] D. Chatterjee, F. Gulminelli, A. R. Raduta, and J. Margueron, Phys. Rev. C **96**, 065805 (2017).
[30] M. Dutra, O. Lourenco, J. S. Sa Martins, A. Delfino, J. R. Stone, and P. D. Stevenson, Phys. Rev. C **85**, 035201 (2012).
[31] D. Vautherin and D. M. Brink, Phys. Rev. C **5**, 626 (1972).
[32] H. S. Kohler, Nucl. Phys. A **258**, 301 (1976).
[33] J. Friedrich and P.-G. Reinhard, Phys. Rev. C **33**, 335 (1986).
[34] L. Bennour, P.-H. Heenen, P. Bonche, J. Dobaczewski, and H. Flocard, Phys. Rev. C **40**, 2834 (1989).
[35] E. Chabanat, Interactions effectives pour des conditions extremes d'isospin, Ph.D. thesis, University Claude Bernard Lyon-1, Lyon, France, 1995 (unpublished).
[36] E. Chabanat, P. Bonche, P. Haensel, J. Meyer, and R. Schaeffer, Nucl. Phys. A **635**, 231 (1998).
[37] E. Chabanat, P. Bonche, P. Haensel, J. Meyer, and R. Schaeffer, Nucl. Phys. A **627**, 710 (1997).
[38] P.-G. Reinhard and H. Flocard, Nucl. Phys. A **584**, 467 (1995).
[39] W. Nazarewicz, J. Dobaczewski, T. R. Werner, J. A. Maruhn, P.-G. Reinhard, K. Rutz, C. R. Chinn, A. S. Umar, and M. R. Strayer, Phys. Rev. C **53**, 740 (1996).
[40] P.-G. Reinhard, D. J. Dean, W. Nazarewicz, J. Dobaczewski, J. A. Maruhn, and M. R. Strayer, Phys. Rev. C **60**, 014316 (1999).
[41] B. K. Agrawal, S. Shlomo, and V. Kim Au, Phys. Rev. C **68**, 031304 (2003).
[42] B. K. Agrawal, S. Shlomo, and V. K. Au, Phys. Rev. C **72**, 014310 (2005).
[43] J. M. Lattimer and Y. Lim, Astrophys. J. **771**, 51 (2013).
[44] M. Fortin, C. Providência, Ad. R. Raduta, F. Gulminelli, J. L. Zdunik, P. Haensel, and M. Bejger, Phys. Rev. C **94**, 035804 (2016).
[45] S. Goriely, N. Chamel, and J. M. Pearson, Phys. Rev. C **88**, 061302(R) (2013).
[46] M. Brack, C. Guet, and H.-B. Hakansson, Phys. Rep. **123**, 275 (1985).
[47] M. Onsi, A. K. Dutta, H. Chatri, S. Goriely, N. Chamel, and J. M. Pearson, Phys. Rev. C **77**, 065805 (2008).
[48] R. B. Wiringa, V. Fiks, and A. Fabrocini, Phys. Rev. C **38**, 1010 (1988).
[49] P. Papakonstantinou, J. Margueron, F. Gulminelli, and Ad. R. Raduta, Phys. Rev. C **88**, 045805 (2013).
[50] F. Aymard, F. Gulminelli, and J. Margueron, J. Phys. G **43**, 045106 (2016).
[51] G. Audi, M. Wang, A. H. Wapstra, F. G. Kondev, M. MacCormick, X. Xu, and B. Pfeiffer, Chin. Phys. C **36**, 1287 (2012); M. Wang, G. Audi, A. H. Wapstra, F. G. Kondev, M. MacCormick, X. Xu, and B. Pfeiffer, *ibid.* **36**, 1603 (2012).
[52] K. Marinova and I. Angeli, ADNDT **99**, 69 (2013).
[53] C. J. Horowitz, Z. Ahmed, C.-M. Jen, A. Rakhman, P. A. Souder, M. M. Dalton, N. Liyanage, K. D. Paschke, K. Saenboonruang, R. Silwal *et al.*, Phys. Rev. C **85**, 032501(R) (2012).
[54] F. Buchinger, J. E. Crawford, A. K. Dutta, J. M. Pearson, and F. Tondeur, Phys. Rev. C **49**, 1402 (1994).
[55] Z. Patyk, A. Baran, J. F. Berger, J. Dechargé, J. Dobaczewski, P. Ring, and A. Sobiczewski, Phys. Rev. C **59**, 704 (1999).
[56] M. Centelles, X. Roca-Maza, X. Vinas, and M. Warda, Phys. Rev. C **82**, 054314 (2010).
[57] M. Warda, X. Viñas, X. Roca-Maza, and M. Centelles, Phys. Rev. C **80**, 024316 (2009).
[58] P. Van Isacker, M. A. Nagarajan, and D. D. Warner, Phys. Rev. C **45**, R13 (1992).
[59] V. Baran, M. Colonna, M. Di Toro, A. Croitoru, and D. Dumitru, Phys. Rev. C **88**, 044610 (2013).
[60] A. Krasznahorkay, M. Csatlos, L. Stuhl, A. Algora, J. Gulyas, J. Timar, N. Paar, D. Vretenar, and M. N. Harakeh, Acta Phys. Pol. B **44**, 559 (2013).
[61] A. Krasznahorkay, N. Paar, D. Vretenar, and M. N. Harakeh, Phys. Lett. B **720**, 428 (2013).
[62] L.-G. Cao, X. Roca-Maza, G. Colo, and H. Sagawa, Phys. Rev. C **92**, 034308 (2015).
[63] X. Roca-Maza, M. Brenna, G. Colo, M. Centelles, X. Vinas, B. K. Agrawal, N. Paar, D. Vretenar, and J. Piekarewicz, Phys. Rev. C **88**, 024316 (2013).
[64] J. P. Blocki, A. G. Magner, P. Ring, and A. A. Vlasenko, Phys. Rev. C **87**, 044304 (2013).
[65] K. Kolehmainen, M. Prakash, J. M. Lattimer, and J. R. Treiner, Nucl. Phys. A **439**, 535 (1985).
[66] M. Centelles, M. Del Estal, and X. Vinas, Nucl. Phys. A **635**, 193 (1998).
[67] J. Treiner and H. Krivine, Ann. Phys. **170**, 406 (1986).
[68] B. A. Brown, Phys. Rev. Lett. **119**, 122502 (2017).
[69] J. Yang and J. Piekarewicz, Phys. Rev. C **97**, 014314 (2018).
[70] X. Roca-Maza, X. Vinas, M. Centelles, B. K. Agrawal, G. Colo, N. Paar, J. Piekarewicz, and D. Vretenar, Phys. Rev. C **92**, 064304 (2015).
[71] P.-G. Reinhard and W. Nazarewicz, Phys. Rev. C **93**, 051303(R) (2016).